IEEE Access
Multidisciplinary | Rapid Review | Open Access Journal

Date of publication xxxx 00, 0000, date of current version xxxx 00, 0000.

Digital Object Identifier 10.1109/ACCESS.2017.DOI

Fast corner detection using approximate form of second-order Gaussian directional derivative

TIAN GAO[1], JUNFENG JING[1], CHAO LIU[1], WEICHUAN ZHANG[2,3] (MEMBER, IEEE), YONGSHENG GAO[2] (SENIOR MEMBER, IEEE), CHANGMING SUN[3]

[1]College of Electrical and Information, Xi'an Polytechnic University, Xi'an, 710048, China. (e-mail: gaotian970228@163.com; jingjunfeng0718@sina.com; 2546458647@qq.com)
[2]The Institute for Integrated and Intelligent Systems, Griffith University, QLD, Australia. (e-mail: yongsheng.gao@griffith.edu.au)
[3]CSIRO Data61, PO Box 76, Epping, NSW 1710, Australia. (e-mail: changming.sun@csiro.au)

Corresponding author: Weichuan Zhang (e-mail: zwc2003@163.com)

This work was supported in part by the Youth Innovation Team of Shaanxi Universities and in part by the Scientific Research Program Funded by the Shaanxi Provincial Education Department under Grant 19JC018.

ABSTRACT High-efficiency image corner detection, one of the most important and critical basic technology in industrial image processing, is to detect point features from an input image in real-time. In this paper, we propose a new corner detection method which has both good performance of corner detection and real-time processing abilities. Firstly, the integral image and the box filter are combined to obtain the second-order derivative response in each direction of the image. Secondly, a new coarse screening mechanism for candidate corners is presented to reduce the complexity of the corner metric. Thirdly, a non-maximum suppression operation is utilized to obtain corners. Finally, the performance evaluation on accuracy of corner detection, localization error, average repeatability, region repeatability, different lighting conditions, and execution time are used to assess the proposed method against twelve state-of-the-art methods. The experimental results show that our proposed detector has good corner detection performance and achieves the requirement of real-time processing.

INDEX TERMS Corner detection, real-time processing, directional derivative, detection performance.

I. INTRODUCTION

CORNERS are one of the most important local features in an image, which have been widely applied in many computer vision and image processing tasks such as 3D reconstruction [1], autonomous driving [2], object recognition [3], and image registration [4]. The existing corner detection methods can be divided into three categories [5]: contour-based [6]–[11], template-based [12]–[15], and intensity-based [5], [16]–[27]. Contour-based methods usually firstly extract edge contours from an input image by an edge detector [28]–[30], and then the information of shape changes on contours are analysed for detecting corners.

Template-based methods find corners by fitting a small patch of an image with predefined corner templates. Smith and Brady [12] used the similarity ratio information between image and smallest univalue segment assimilating nucleus (SUSAN) template to detect corners. Rosten et al. [13], [14] followed the SUSAN method [12] and applied a decision tree technique to detect corners. Su et al. [31] applied the Hessian matrix and correlation matrix of an image to detect candidate junctions. And then the average intensity in all directions, and the zero-mean normalized cross correlation were utilized to improve the accuracy of junction detection. Xia et al. [15] presented an interest point detector based on the change of edge pixel intensity in a linear scale space. Xue et al. [32] extended the Xia et al.'s method [15] that junctions are detected from edge contours in a nonlinear scale space.

Following Moravec's definition [16] that the intensity variations of corners are large in all directions, Harris and Stephens [17] utilized first-order image derivatives along the horizontal and vertical directions to construct a 2×2 structure tensor for detecting corners from an input image. Subsequently, multi-scale technique [33], log-Gabor filter [34], and shearlet filter [23] are applied to smooth the input image and extract corners in the framework of the Harris method.

This article has been accepted for publication in a future issue of this journal, but has not been fully edited. Content may change prior to final publication. Citation information: DOI 10.1109/ACCESS.2020.3032751, IEEE Access

Zhang and Sun [5], [27] showed that it is necessary to extract local structure information of corners from an input image along multiple filter orientations. The reason is that the first- or second-order directional derivatives along a pair of orthogonal directions cannot properly identify the differences between edges and corners. Then Zhang and Sun [27] presented the second-order generalized Gaussian directional derivative (SOGGDD) method for detecting corners from images. In [27], the SOGGDD filters are employed to smooth the input image, and then the second-order directional derivatives along multiple filter orientations are used to construct a second-order directional derivative correlation matrix for detecting corners. Wang et al. [35] applied Zhang and Sun methods [5], [27] and multi-scale shearlet filters with multiple directions are used to smooth the input image for detecting corners.

Lindeberg [18] utilized Laplace-of-Gaussian (LoG) filters to smooth the input image for detecting local features in scale space. Lowe [19] extended the LoG method [18] and presented the scale-invariant feature transform (SIFT) algorithm. Difference of Gaussian (DoG) filters with multiple scales are used to detect local features from images. Bay et al. [20] applied box filters to speed up the execution time of the SIFT method [19]. Alcantarilla et al. [21] applied the anisotropic diffusion theory to construct a nonlinear scale space and extract the maxima of the Hessian in this scale space to detect local features. Hong-Phuoc and Guan [36] utilized a sparse coding method to detect local features. Cho et al. [22] utilized higher-order DoG and LoG filters to detect local features. Verdie et al. [37] presented a model learned by image sets about the same scene with different time and seasons to detect local features. Yi et al. [38] employed traditional detectors such as SIFT [19] to train their local feature detector. Lenc and Vedaldi [39] trained a feature detector by the local covariant constraint. Ono et al. [40] applied interest points with high repeatability to train a local feature detector. Dusmanu et al. [41] applied the response from the pre-trained VGG-16 to detect local features.

Our research indicates that the detector proposed by Zhang and Sun [27] has the ability to properly extract the local structure information from each input image for detecting corners. However, its computational complexity is very high and cannot meet the requirements of real-time processing. Inspired by the SURF method [20], the integral image and box filter are combined to approximate the second-order Gaussian directional derivative (SOGDD) filters. In this way, the time complexity of the convolution operation can be reduced from $O(N^2)$ (N represents the size of the convolution template) to $O(1)$. Furthermore, a mechanism that filters out candidate corners was proposed to reduce the time consumption of the process about constructing the image corner measure map. Finally, the performance evaluation on the accuracy of corner detection, localization error, average repeatability, region repeatability, and execution time are used to assess the proposed method against twelve state-of-the-art methods. The experimental results show that our proposed detector has good corner detection performance and achieves the requirement of real-time processing.

The remainder of the article is arranged as follows. In Section II, a succinct review of second-order Gaussian directional derivative filter and detailed introduction of our proposed corner detector are provided. In Section III, the performances for the thirteen state-of-the-art approaches based on evaluation criteria (detection accuracy, affine transformation [9], region repeatability [42], different lighting conditions, and execution time) are discussed. Finally, a conclusion is presented in Section IV.

II. PROPOSED CORNER DETECTOR

In [5], Zhang and Sun proved that it is necessary for us to extract local structure information along multiple filter orientations from an input image for detecting corners. Our research indicates that convolution operation of multi-directional filtering increases the computational complexity of the SOGGDD algorithm [27], which makes the SOGGDD algorithm unable to meet the needs of real-time corner detection. The goal of this paper is to present a corner detector which has good performance of corner detection and has the ability to meet the requirement of real-time processing.

A. SECOND-ORDER GAUSSIAN DIRECTIONAL DERIVATIVE FILTERS

In this subsection, a brief review of the SOGGDD filter is given. The Gaussian filters $\mathbf{G}_{\sigma,\rho,\varphi}(x,y)$ in continuous domain can be expressed as [5], [27]:

$$\mathbf{G}_{\sigma,\varphi}(x,y) = \frac{1}{2\pi\sigma^2}\exp\left(-\frac{1}{2\sigma^2}[x,y]\Psi_{-\varphi}\begin{bmatrix}\rho^2 & 0\\ 0 & \rho^{-2}\end{bmatrix}\Psi_{\varphi}[x,y]^T\right), \tag{1}$$

with

$$\Psi_{\varphi} = \begin{bmatrix}\cos\varphi & \sin\varphi\\ -\sin\varphi & \cos\varphi\end{bmatrix}$$

where T represents matrix transpose, σ is scale factor, ρ is the anisotropic factor, and Ψ_{φ} is the rotation matrix in orientation φ.

The first-order generalized Gaussian directional derivative filter $\Lambda_{\sigma,\varphi}(x,y)$ with orientation φ is shown as follow:

$$\begin{aligned}\Lambda_{\sigma,\rho,\varphi}(x,y) &= \frac{\partial\mathbf{G}_{\sigma,\rho}}{\partial\varphi}\left(\Psi_{\varphi}[x,y]^{\top}\right)\\ &= -\frac{\rho^2(x\cos\varphi + y\sin\varphi)}{\sigma^2}\mathbf{G}_{\sigma,\rho,\varphi}(x,y),\end{aligned} \tag{2}$$

The SOGGDD filter $\phi_{\sigma,\rho,\varphi}(x,y)$ with orientation φ can be obtained as follow:

$$\begin{aligned}\phi_{\sigma,\rho,\varphi}(x,y) &= \frac{\partial\Lambda_{\sigma,\rho}}{\partial\varphi}\left(\Psi_{\varphi}[x,y]^{\top}\right)\\ &= \frac{\rho^2}{\sigma^2}\left(\frac{\rho^2}{\sigma^2}(x\cos\varphi + y\sin\varphi)^2 - 1\right)\mathbf{G}_{\sigma,\rho,\varphi}(x,y),\end{aligned} \tag{3}$$

This article has been accepted for publication in a future issue of this journal, but has not been fully edited. Content may change prior to final publication. Citation information: DOI 10.1109/ACCESS.2020.3032751, IEEE Access

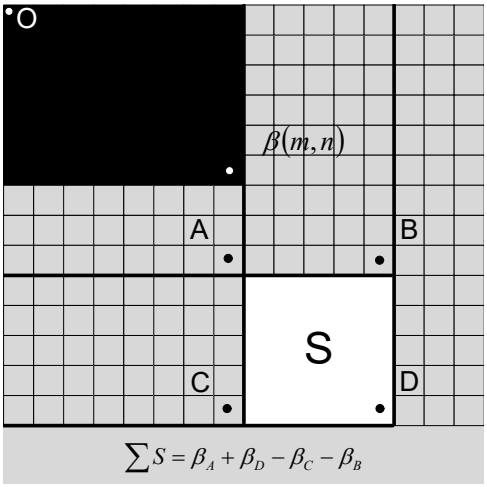

FIGURE 1. Integral image schematic diagram.

It is worth to note that images are 2D discrete signals in the integer grid, which means that the SOGGDD filter should be discretized for performing different image processing tasks. Given a scale σ and K oriented angles $\varphi_k = (k-1)2\pi/K$ $(k = 1, 2, \ldots, K)$, and the location (m, n) in the image, the discrete version of the SOGGDD filters can be represented as:

$$\begin{aligned}&\phi_{\sigma,\rho,\varphi_k}(m,n)\\&= \tfrac{\rho^2}{\sigma^2}\left(\tfrac{\rho^2}{\sigma^2}([\cos\varphi_k, \sin\varphi_k][m,n]^T)^2 - 1\right)\mathbf{G}_{\sigma,\rho,\varphi_k}(m,n),\end{aligned} \tag{4}$$

In the following, the anisotropic factor with $\rho^2 = 1$ and the scale factor with $\sigma^2 = 1.5$ of the second-order Gaussian directional derivative filters are utilized in our proposed method.

B. INTEGRAL IMAGE

In this subsection, we first give a concise review on the integral image [43]. The integral image has the same image resolution as the original image. As shown in Fig. 1, the pixel 'O' represents the first pixel in the upper left corner of the image. The value at position (m, n) in the integral image is the sum of all pixels covered by black region in the original image

$$\beta(m,n) = \sum_{m' \le m,\ n' \le n} I(m', n'), \tag{5}$$

where β represents an integral image, I represents an original image, (m, n) is a pixel position in the integral image, and (m', n') is a pixel position in the original image.

An optimization method is introduced to efficiently calculate the integral image as follows:

$$\begin{aligned}c(m,n) &= c(m,n-1) + I(m,n),\\ \beta(m,n) &= \beta(m-1,n) + c(m,n),\end{aligned} \tag{6}$$

where $c(m, n)$ represents the pixel sum of the column (ending at row m) in the original image.

Once an integral image is obtained, the sum of pixel values of a certain rectangular area in the original image can be obtained by putting three addition operation to the values of the corresponding four positions in the integral image, which is extremely compatible with the box filter in terms of reducing the calculation complexity of an image convolution operation.

As shown in Fig. 1, the pixel sum of the white area S in the original image is calculated

$$S = \beta_A + \beta_D - \beta_C - \beta_B, \tag{7}$$

where β_A, β_B, β_C, and β_D are the values at positions A, B, C, and D in the integral image respectively.

C. BOX FILTER

The existing corner detection algorithms usually apply a predesigned filter to convolve the input image for obtaining multi-directional response of an input image. The process of the convolution operation usually cause high computational cost for image corner detectors. Furthermore, many complex filters (e.g., shearlet filter and log-Gabor filter) are not as separable as Gaussian filters, so they cannot be decomposed into two one-dimensional filter kernels for fast calculation. For a SOGDD convolution template with the size of $N \times N$ pixels, a complete convolution process will include N^2 multiplication operations and $N^2 - 1$ addition operations. For some applications that have high-resolution input images, such as high-resolution remote sensing [44] and astronomical image processing [45], the time consumption of pixel-by-pixel convolution operation is very high.

In this paper, the box filter is applied to approximate complex multi-directional SOGDD filters for detecting corners from an input image. Take a vertical second-order derivative filter template as an example as shown in Fig. 2, an SOGDD filter and a box filter are shown in Fig. 2(a) and (b) respectively. It can be seen from Fig. 2(a) that the weight distribution of the SOGDD filter can be divided into three parts. The weight of the two white areas is greater than 0 and the weight of the black area is less than 0. According to Equation (4) and the properties of the SOGDD filter, it can be found that the absolute value of the weight of the pixels in the black area is twice that of the corresponding pixels in the white area.

In addition, in order to be consistent with the property of integral image that it can efficiently calculate the sum of pixels in the rectangular area, the main area of the second-order Gaussian directional derivative filter template is approximated to three square areas with the size of 3×3 pixels (the selection of template size will be discussed in Section III). As shown in Fig. 2(b), the weights of the black, white, and gray areas are -2, 1, and 0 respectively. Taking into account the needs of real-time detection and the accuracy of corner detection, the box filters with six filter orientations are used in our method. The box filter templates with six filter orientations are shown in Fig. 3.

This article has been accepted for publication in a future issue of this journal, but has not been fully edited. Content may change prior to final publication. Citation information: DOI 10.1109/ACCESS.2020.3032751, IEEE Access

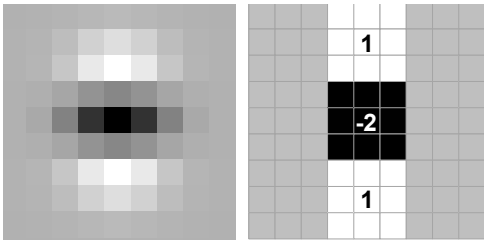

FIGURE 2. One SOGDD filter template in vertical direction in (a) and its corresponding box filter template in (b).

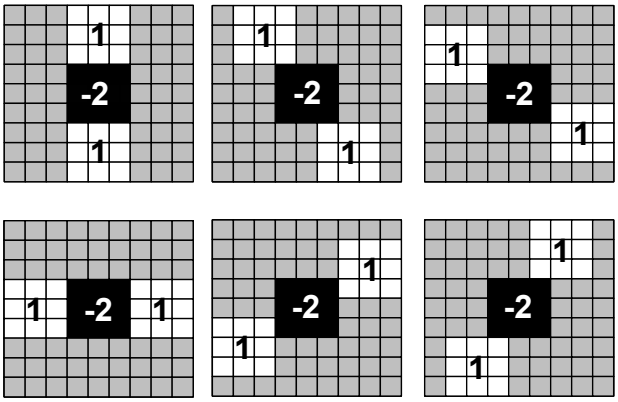

FIGURE 3. The templates of box filter with six filter orientations.

Based on the aforementioned analysis, it can be found that the combination of the integral image and the box filter has the ability to properly obtain the second-order directional derivative information as the SOGGDD method [27] does. Furthermore, the combination of the integral image and the box filter has the ability to meet the requirement of real-time processing. As shown in Fig. 1 and Fig. 2(b), for one image pixel, only $3\times3+2$ addition operations are required to obtain the SOGDD information along one direction in our proposed method. The computational complexity of the box filter and the SOGDD filter with six filter orientations (the size of the template is $N \times N$ pixels) are shown in Table 1.

TABLE 1. The comparison of the computational complexity between the box filter and the original filter.

Filter	Addition operation	Multiplication operation	Total operation
SOGDD	$6 \times (N^2 - 1)$	$6N^2$	$6 \times (2N^2 - 1)$
Box	$6 \times (3 \times 3 + 2) - 15$	0	51

It can be seen from Table 1 that the computational complexity of the box filter to obtain the second-order directional derivative from one image pixel is $O(1)$, while the computational complexity of the SOGDD filter [27] to obtain the second-order directional derivative from one image pixel is $O(N^2)$. And when the size of the SOGDD filter template increases, the acceleration effect of the box filter will become more apparent.

D. ROUGH SCREENING FOR CANDIDATE CORNER SET BASED ON SUM OF DIRECTIONAL DERIVATIVES

Our research indicates that the corner measurement map constructed by the SOGGDD algorithm [27] is very complex. For one pixel in the input image, there are $49 \times 49 + 5$ multiplication operations, $48 \times 48 + 6$ addition operations, one division operation, 2×49 memory access operations, and one operation about finding the eigenvalue of a matrix to obtain the corner measure. Meanwhile, the detector needs to apply this operation on all pixels of the input image to obtain the corner measurement map of the entire image, which undoubtedly increases the computational complexity of the detector to an extremely high level. However, the sparseness of corners indicates that the method which calculates corner measure pixel by pixel is extremely inefficient. In our proposed method, a method that pre-screens candidate points from the whole image was proposed to reduce the number of operations for calculating the corner measure. Following the corner definition proposed in [5], a corner is the point where the pixel value derivative is large in multiple directions, we can utilize the sum of multi-directional derivative values to filter out candidate corner point set.

In our method, we preset an appropriate threshold to compare with the sum of multi-directional derivatives of each pixel in the input image. In this way, we only need performing five summation operations and one comparison operation for each pixel to reduce the computational complexity for obtaining corner measures by orders of magnitude. After the coarse screening process, only a small number of pixels are needed to construct the second-order directional derivative correlation matrix to carry out further screening. For an input image with the size of $W \times V$, the corner number of candidate corner set is CC and $CC \ll W \times V$. The comparison between our corner detector applying a rough screening method and the detector applying a pixel-by-pixel traversal method on the computation complexity for computing the corner measure map is shown in Table 2 (the image direction derivative response has been obtained), which shows that our method greatly improves the running speed of obtaining the cornerness map of an input image. In our method, the threshold for the rough screening processing was set as $3\times T_h$ (the selection of threshold will be discussed in Section III.) and T_h means the average value of the sum of the multi-directional derivatives of all pixels in the input image.

E. CONSTRUCT MULTI-DIRECTIONAL CORNER STRUCTURE TENSOR PRODUCT

The three areas in the pre-designed box filter template as shown in Fig. 2(b) are denoted as area X, area Y, and area Z from top to bottom respectively. Meanwhile, corresponding image location of the center point of the three areas are denoted as (X_m, X_n), (Y_m, Y_n), and (Z_m, Z_n) respectively. The sum of the pixel values of the image region covered by

This article has been accepted for publication in a future issue of this journal, but has not been fully edited. Content may change prior to final publication. Citation information: DOI 10.1109/ACCESS.2020.3032751, IEEE Access

TABLE 2. The computational complexity of our method with rough screening and without rough screening in the cornerness map calculation.

Method	Addition operation	Multiplication operation	Division operation	Finding eigenvalues of the SODDC matrix
Without rough screening	$(5+48+6)\times WV$	$WV\times(7\times7+5)$	WV	WV
Rough screening	$5\times(WV-CC)+(48+6)\times CC$	$CC\times(7\times7+5)$	CC	CC

area X is defined as S_X, which is shown as follow:

$$S_X=\beta(X_m-2,X_n-2)+\beta(X_m+1,X_n+1) -\beta(X_m+1,X_n-2)-\beta(X_m-2,X_n+1). \tag{8}$$

The sums of the pixel values of the regions covered by area Y and area Z are defined as S_Y and S_Z, which have the same form with Equation (8). In this way, the second-order Gaussian directional derivative $\nabla_k I(Y_m,Y_n)$ of pixel $I(Y_m,Y_n)$ (the center point of the black area is also the center point of the convolution template) in the k-th ($k=1,2,\ldots,K$)) direction is defined as:

$$\nabla_k I(Y_m,Y_n)=S_X+S_Z-2S_Y. \tag{9}$$

Following the SOGGDD algorithm [27], the second-order directional derivative correlation (SODDC) matrix is constructed for each image pixel, which is given in Equation (10). In Equation (10), $(m+i,n+j)$ is a point in a neighbourhood within a certain range centered on (m,n) and (i,j) is within the region of a rectangular window. Then, the corresponding eigenvalues $\{\lambda_1,\lambda_2,\ldots,\lambda_K\}$ of the SODDC matrix M are obtained to construct a corner measure Ω.

$$\Omega(m,n)=\frac{\prod_{k=1}^{K}\lambda_k}{\sum_{k=1}^{K}\lambda_k+\epsilon}, \tag{11}$$

where ϵ is a tiny constant $\left(\epsilon=1\times10^{-16}\right)$ which is used to avoid a singular denominator. Finally, the pixel that has a local maxima value on the corner measure map and is larger than a threshold T is marked as a corner.

The outline of the proposed corner detection method is summarized as follow:

1) Calculating the integral image of the input image by Equation (6).
2) Applying a box filter bank to approximate the SOGDD filter with multiple directions and obtaining the image second-order directional derivative information.
3) Screening candidate corners by the sum of directional derivative in all directions.
4) Constructing the SODDC matrix and calculating the corner measure Ω for each candidate corner.
5) Integrating Ω of all pixels in the input image (the Ω of the pixel that is not candidate corner is set to 0) to obtain a corner measure map (CMP).
6) Applying the non-maximum suppression technique on CMP to obtain corners.

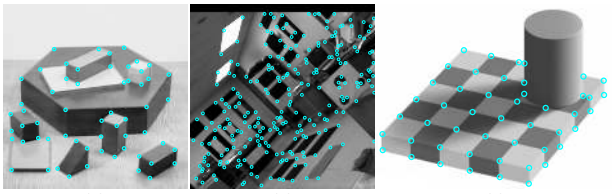

FIGURE 4. The ground truth of corner positions in three test image. (a), (b), and (c) are the image 'Block', 'Lab', and 'Checkerboard' respectively.

III. PERFORMANCE EVALUATION

In this section, six performance evaluation criteria (accuracy of corner detection [27], localization error [27], average repeatability under image affine transformation [9], region repeatability [42], execution time, and different lighting conditions) are utilized to evaluate the performance for our proposed method and twelve state-of-the-art detectors (Harris [17], Harris-Laplace [33], ANDD [46], ACJ [15], SOGGDD [27], DoG [19], SURF [20], D2-Net [41], LF-Net [40], New-Curvature [11], Gabor [47], and NRANDD [10]). The codes for ANDD [46], ACJ [15], SOGGDD [27], D2-Net [41], LF-Net [40], New-Curvature [11], Gabor [47], and NRANDD [10] come from authors. The codes for Harris-Laplace [33] and DoG [19] are from [48]. The codes for SURF [20] and Harris [17] are from MATLAB and [49] respectively.

A. EVALUATION OF DETECTION PERFORMANCE BASED ON GROUND TRUTHS

In this subsection, the criteria on accuracy of detection and location error [27] are used to evaluate the performance of the thirteen methods. Three test images 'Block' [50], 'Lab' [50], and 'Checkerboard' [15] and their corresponding ground truth (marked by cyan circle) are shown in Fig. 4. The three test images 'Block', 'Lab', and 'Checkerboard' contain 59, 249, and 50 corners respectively. The ground truths of 'Block' and 'Lab' come from [10] and the ground truth of 'Checkerboard' is manually marked as described in [51]. Ten experts are invited to mark corners for test image 'Checkerboard'. Only when a corner is marked by at least eight experts at the time will it be considered as a ground truth corner for the image 'Checkerboard'.

Let $\tau_{\text{detected}}=\{(\hat{r}_p,\hat{c}_p),\quad p=1,2,\ldots,N_1\}$ refer to the corner set detected by a corner detector and $\tau_{\text{truth}}=\{(r_q,c_q),\quad q=1,2,\ldots,N_2\}$ refer to the corner set contained in the ground truth data. For a corner (r_q,c_q) selected from the ground truth corner set, If there exists a corner $(\hat{r}_p,\hat{c}_p)$ that belongs to the detected corner set which is not

This article has been accepted for publication in a future issue of this journal, but has not been fully edited. Content may change prior to final publication. Citation information: DOI 10.1109/ACCESS.2020.3032751, IEEE Access

$$M = \begin{bmatrix} \sum_{i=-\frac{u}{2}}^{\frac{u}{2}} \sum_{j=-\frac{v}{2}}^{\frac{v}{2}} \nabla_1^2 I(m+i,n+j) & \cdots & \sum_{i=-\frac{u}{2}}^{\frac{u}{2}} \sum_{j=-\frac{v}{2}}^{\frac{v}{2}} \nabla_1 I(m+i,n+j) \nabla_K I(m+i,n+j) \\ \vdots & \ddots & \vdots \\ \sum_{i=-\frac{u}{2}}^{\frac{u}{2}} \sum_{j=-\frac{v}{2}}^{\frac{v}{2}} \nabla_1 I(m+i,n+j) \nabla_K I(m+i,n+j) & \cdots & \sum_{i=-\frac{u}{2}}^{\frac{u}{2}} \sum_{j=-\frac{v}{2}}^{\frac{v}{2}} \nabla_K^2 I(m+i,n+j) \end{bmatrix}, \tag{10}$$

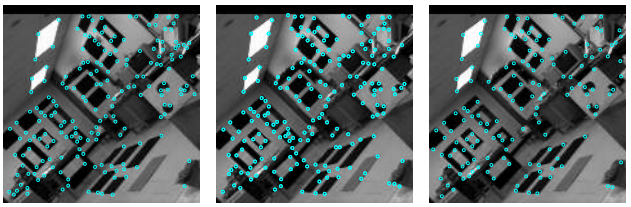

(a) (b) (c)

FIGURE 5. Detection results on the test image 'Lab'. (a)Range size with 3×3, (b) Range size with 5×5, (c) Range size with 7×7.

more than 4 pixels away from (r_q, c_q), a true matching corner pair is obtained and the corner $(\hat{r}_p, \hat{c}_p)$ will be considered as a true corner. Otherwise, the corner (r_q, c_q) will be considered as a missing point. If the detected corner $(\hat{r}_p, \hat{c}_p)$ is far away from the ground truth, the corner $(\hat{r}_p, \hat{c}_p)$ will be considered as a false corner. Meanwhile, the localization error of the detected corner is also an important metric to evaluate the detection accuracy of a corner detector. Let $\{(\hat{r}_i, \hat{c}_i), (r_i, c_i) : i = 1, 2, \ldots, M\}$ be the matching pair obtained from sets τ_{detected} and τ_{truth}, then the average localization error can be calculated as:

$$L_d = \sqrt{\frac{1}{M} \sum_{i=1}^{M} \left((\hat{r}_i - r_i)^2 + (\hat{c}_i - c_i)^2 \right)}. \tag{12}$$

Test image 'Lab' [50] is used to illustrate the effect of the filter template size on the accuracy of corner detection. The corner detection results using a box filter with different template sizes (i.e., 3×3, 5×5, and 7×7) are shown in Fig. 5. The accuracy of corner detection and localization error are summarized in Table 3. It can be found from Table 3 that the box filter with a 3×3 template size achieves the best accuracy of corner detection and the smallest localization error. In this way, the box filter with a 3×3 template size is selected in our method.

TABLE 3. Performance comparison for the proposed detectors with different range sizes.

Range size	Missed corners	False corners	Localization error (pixel)
3×3	103	43	1.429
5×5	104	57	2.270
7×7	150	55	3.286

Our research indicates that an effective threshold of rough screening can reduce the computational complexity of the algorithm while not causing loss of corner detection accuracy. Take test image 'Lab' [50] as an example, its corresponding corner detection accuracy and execution time with different rough screening thresholds are illustrated in Table 4. It can be seen that when the threshold of rough screening is $3 \times T_h$ (T_h is the average of the sum of the multi-directional derivatives of all pixels in an input image), the proposed method achieves the smallest localization error, the second-best accuracy of corner detection, and relatively short execution time. In this way, $3 \times T_h$ is selected as the threshold for rough screening processing.

TABLE 4. Performance comparison for the proposed method with different rough screening thresholds.

Threshold ($* \times Th$)	Missed corners	False corners	Localization error (pixel)	Execution time (s)
1	105	44	1.448	0.535
2	104	42	1.472	0.420
3	103	43	1.428	0.358
4	100	44	1.522	0.312
5	111	41	1.588	0.286
6	135	30	1.852	0.274

The results of corner detection of our method and five other corner detectors (Harris [17], ACJ [15], Harris-Laplace [33], ANDD [46], and SOGGDD [27]) on three test images are shown in Fig. 6, Fig. 7, and Fig. 8 respectively. The numbers of missed corners, false corners, and average location distance error for all methods are shown in Table 5. In this evolution, the threshold of all detectors was set as the value which can make the number of detected corners suitable for the ground truth. For our method, the threshold for corner measure was set to 10^{25}.

In this evaluation, both the missed corners and false corners are used to assess the performance of each detection method. As shown in Table 5, the numbers of missed corners and false corners for Harris [17], ACJ [15], Harris-Laplace [33], ANDD [46], SOGGDD [27], and our proposed method for the test image 'Block' are '21', '10', '76', '9', '11', and '10' respectively. For the test image 'Lab', the numbers of missed corners and false corners for the six detectors are '175', '149', '383', '152', '163', and '146'

This article has been accepted for publication in a future issue of this journal, but has not been fully edited. Content may change prior to final publication. Citation information: DOI 10.1109/ACCESS.2020.3032751, IEEE Access

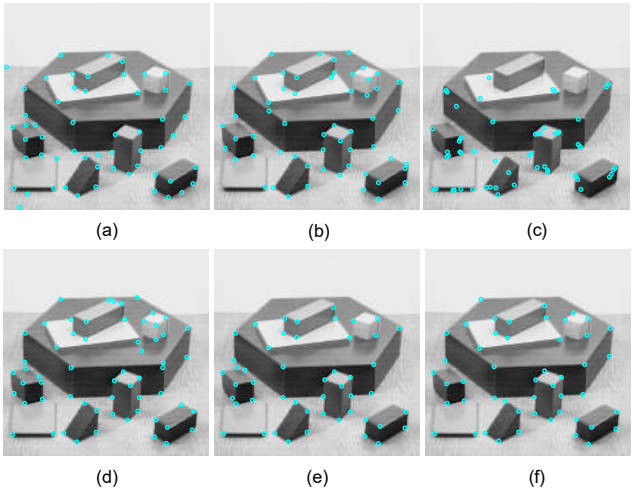

FIGURE 6. Detection results on the test image 'Block'. (a) Harris [17], (b) ACJ [15], (c) Harris-Laplace [33], (d) ANDD [46], (e) SOGGDD [27], and (f) Proposed detector.

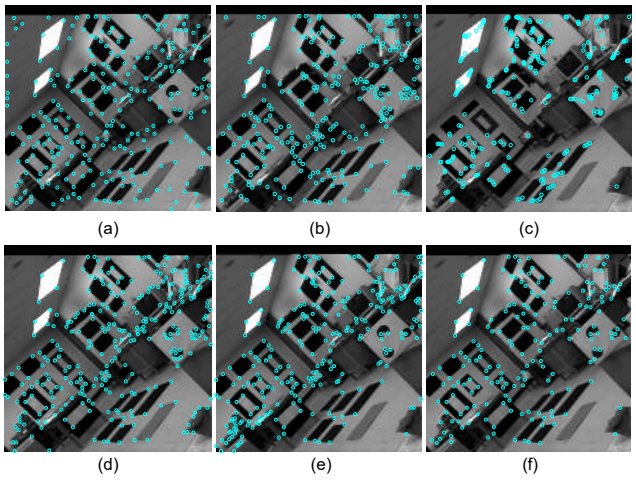

FIGURE 7. Detection results on the test image 'Lab'. (a) Harris [17], (b) ACJ [15], (c) Harris-Laplace [33], (d) ANDD [46], (e) SOGGDD [27], and (f) Proposed detector.

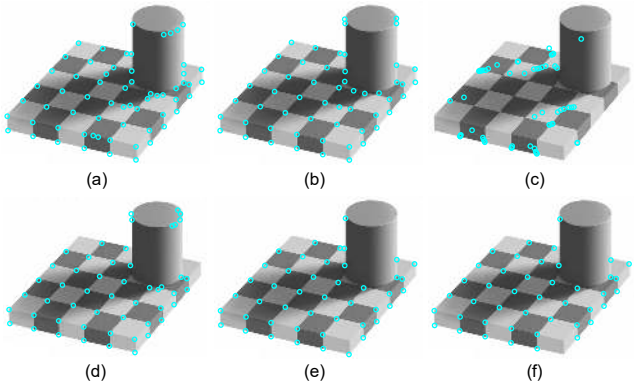

FIGURE 8. Detection results on the test image 'Checkerboard'. (a) Harris [17], (b) ACJ [15], (c) Harris-Laplace [33], (d) ANDD [46], (e) SOGGDD [27], and (f) Proposed detector.

respectively. For the image 'Checkerboard', the numbers of

TABLE 5. Performance comparison for the six detectors on three ground truth test images.

Method	Missed corners	False corners	Localization error (pixel)
image 'Block'			
Harris	12	9	1.732
ACJ	6	4	1.660
Harris-Laplace	38	38	2.400
ANDD	**4**	5	1.763
SOGGDD	12	2	**1.488**
Proposed	10	**0**	1.558
image 'Lab'			
Harris	84	91	1.573
ACJ	77	72	2.009
Harris-Laplace	175	208	2.941
ANDD	**57**	95	1.625
SOGGDD	72	91	1.461
Proposed	103	**43**	**1.429**
image 'Checkerboard'			
Harris	**0**	15	1.400
ACJ	**0**	7	1.323
Harris-Laplace	36	42	2.141
ANDD	6	9	1.760
SOGGDD	5	**0**	1.137
Proposed	6	1	**0.913**

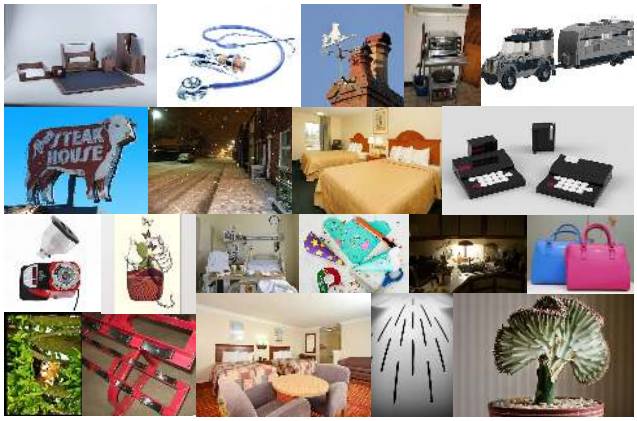

FIGURE 9. Test image set for the evaluation about repeatability under image transformation.

missed corners and false corners for the six detectors are 15', '7', '78', '15', '5', and '7' respectively. For the localization error metric, our method attains the smallest location error for three test images. Benefiting from the extraction of multi-directional derivative information, the double screening on multi-directional derivative sum, and multi-directional structure tensor product, our method achieves good detection performance.

This article has been accepted for publication in a future issue of this journal, but has not been fully edited. Content may change prior to final publication. Citation information: DOI 10.1109/ACCESS.2020.3032751, IEEE Access

B. REPEATABILITY UNDER IMAGE TRANSFORMATION

In [9], the average repeatability metric R_{epeat} precisely measures the affine robustness, noise stability, and JPEG compression invariance of the corner detector through the local features extracted from original and transformed images, which is calculated as follows:

$$R_{\text{epeat}} = \frac{Num_{matched}}{2}\left(\frac{1}{Num_{ori}} + \frac{1}{Num_{trans}}\right), \quad (13)$$

where Num_{ori} and Num_{trans} represent the count of extracted corners from the original image 'I' and transformed image 'J' respectively, and $Num_{matched}$ is the number of the matched corner pairs extracted from images 'I' and 'J'.

The transformation relationship between the original and affine transformed images is already determined when generating the transformed image, which avoids the error caused by calculating the homography matrix between the images, and the evaluation criteria can be adapted to any image. The rule of determining a true match corner pair is defined as follow: Firstly, we define two corners $C_o = (x_o, y_o)$ and $C_t = (x_t, y_t)$ which are detected in the original image and transformed image respectively. Secondly, if the position of corner C_o after image transformation is in the neighbourhood of C_t (the distance between the two corners does not exceed 4 pixels), then a matched corner pair is obtained.

There are 20 images with different scenes from the ImageNet dataset [52] (shown in Fig. 9) which are utilized to measure the average repeatability of the interest point detectors. We followed the standard criteria proposed in [53] that a total of 4,340 transformed test images were obtained by applying the following six different types of transformations on each original image:

• Rotation: Except for angle 0, the original image is rotated by angle $\pi/18$ in the range $[-\pi/2, \pi/2]$ to obtain a test image.

• Uniform scaling: The image resolution factor in horizontal and vertical direction are defined as σ_x and σ_y respectively. Except for 1, resolution factor in both directions change simultaneously in the range of $[0.5, 2]$ with 0.1 apart.

• Non-uniform scaling: Except the situation $\sigma_x = \sigma_y$, the factor σ_x is changed in the range of $[0.7, 1.5]$ and σ_y is in $[0.5, 1.8]$ with 0.1 apart.

• Shear transformations: Except the situation $S_h = 0$, the shear factor S_h was changed in the range $[-1, 1]$ with 0.1 apart. The image was transformed with the following formula

$$\begin{bmatrix} r' \\ c' \end{bmatrix} = \begin{bmatrix} 1 & S_h \\ 0 & 1 \end{bmatrix} \begin{bmatrix} r \\ c \end{bmatrix}$$

• Lossy JPEG compression: The compression factor is changed in the range of $[5, 100]$ with 5 apart.

• Gaussian noise: The standard deviations of zero mean white Gaussian noise which was added to the original image was changed in the range of $[1, 15]$ with 1 apart.

The experimental results of the thirteen detector are shown in Fig. 10 and sumarized in Table 6. It can be found from Table 6 that our proposed method achieves the second best performance in image affine transformations.

C. REPEATABILITY SCORE UNDER REGION REPEATABILITY EVALUATION

In [42], three parameters of the elliptic implicit equation are applied to describe the range of the corresponding area of the image covered by the features. A region overlap based evaluation criterion and the Oxford database about naturally textured scenes were proposed. For a given corresponding image pairs, the ratio for the number of matched interest point pairs and detected smaller region number in one of the images is defined as the repeatability score. It is depicted as:

$$Re_{\text{i}} = \frac{\mathbf{IPP}_{1i}}{\min(\mathbf{IP}_1, \mathbf{IP}_i)} \quad (i = 1, 2, \ldots, 6), \quad (14)$$

where the $\mathbf{IPP}_{1i}$ is the number of interest point pair detected in the original image and i-th transformation image. And the $\mathbf{IP}_1$ is the number of interest point detected in the original image. Meanwhile, $\mathbf{IP}_i$ is the interest point number detected in the i-th transformation image. A successful match was determined when the overlap error of the interest point pair is below 40 percent. And the overlap error is defined as :

$$\nu = 1 - \frac{R_a \cap H^T R_b H}{R_a \cup H^T R_b H}, \quad (15)$$

where R_a represents the feature in the original image, R_b is the corresponding interest point in the image after transformation and H is the corresponding homography matrix between the original image and the image after transformation. H^T means the transpose matrix for H. To test the accuracy of feature matching, the matching score defined as the ratio between the number of correct matches and the smaller number of detected regions in the pair of images was proposed. In this evaluation, we search six scenes ('Bark' and 'Boat' was deleted) from all eight image scenes ('Bark', 'Bikes', 'Boat', 'Graffiti', 'Leuven', 'Trees', 'Ubc', and 'Wall') in the Oxford image database. The threshold for each method is tuned to extract about 1,000 interest points from each input image. The repeatability scores for the six image sequences are illustrated in Fig. 11 and Table 7.

D. REPEATABILITY SCORE UNDER DIFFERENT LIGHTING CONDITIONS

In this subsection, six image scenes ('Metz', 'Notredame14' (N14), 'Notredame15' (N15), 'Riga', 'Trevi02', and 'Vatican') selected from the Symbench dataset [54] are used to assess the robustness to the illumination changes of corner detectors using the evaluation criteria proposed in [42]. The threshold for each method is tuned to extract about 1,500 corners from each image. The repeatability scores for each detector are illustrated in Fig. 12 and Table 8. It can be observed that our proposed method achieves the second-best performance in images with different lighting conditions.

This article has been accepted for publication in a future issue of this journal, but has not been fully edited. Content may change prior to final publication. Citation information: DOI 10.1109/ACCESS.2020.3032751, IEEE Access

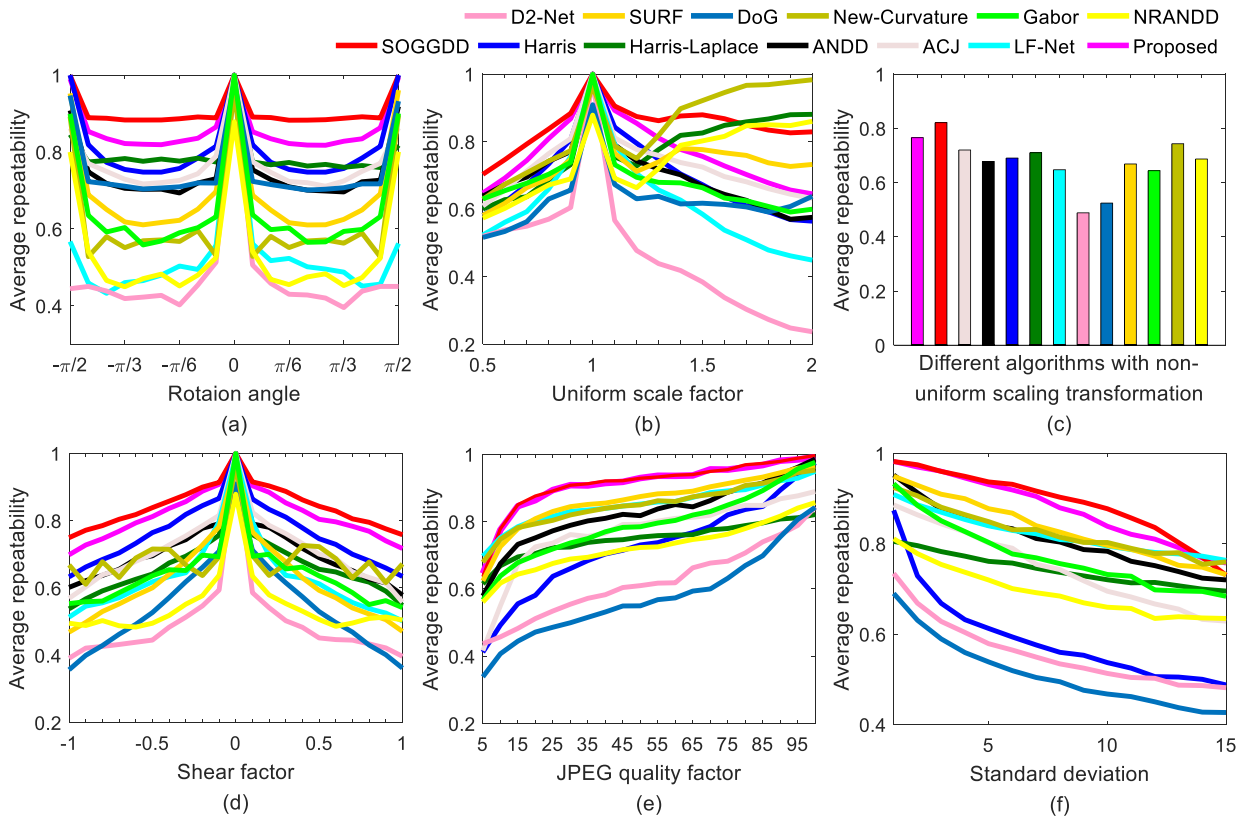

FIGURE 10. Average repeatability under image transformation for thirteen detectors.

TABLE 6. Average result for repeatability under image transformation.

Detector	Rotation	Uniform scale	Non-uniform scale	Shear	JPEG compression	Gaussian noise	Average
ACJ	0.768	0.730	0.720	0.708	0.769	0.746	0.740
ANDD	0.752	0.697	0.678	0.705	0.827	0.810	0.745
Harris	0.796	0.697	0.690	0.759	0.726	0.591	0.710
Harris- Laplace	0.791	0.782	0.710	0.666	0.749	0.742	0.740
LF-Net	0.525	0.618	0.647	0.631	0.852	0.820	0.682
D2-Net	0.470	0.467	0.488	0.494	0.622	0.557	0.516
SURF	0.694	0.736	0.668	0.620	0.862	0.833	0.736
DoG	0.750	0.628	0.525	0.542	0.578	0.512	0.590
New-Curvature	0.617	0.844	0.743	0.686	0.850	0.825	0.761
Gabor	0.651	0.682	0.644	0.638	0.792	0.772	0.697
NRANDD	0.538	0.746	0.687	0.544	0.725	0.694	0.656
SOGGDD	**0.895**	**0.848**	**0.821**	**0.842**	**0.912**	**0.888**	**0.868**
Proposed	0.860	0.772	0.766	0.815	**0.912**	0.876	0.833

E. EXECUTION TIME

In this evaluation criteria, each corner detector has been implemented in MATLAB (R2016b) using a 2.20 GHz CPU with 8 GB of memory. Seven images ('Block', 'Lab', 'Boat', 'Polygon', 'Checkerboard', 'Bikes', and 'Tree') are selected to evaluate the execution time of each detector. Images 'Boat', 'Bikes', and 'Tree' come from the VGG dataset [42] and images 'Lab', 'Block', 'Polygon', and 'Checkerboard' come from [15]. Each image is used for running 100 times to find the average execution time for each detector. The average execution time comparisons are sumarized in Table 9. It can be found from Table 9 that our method achieves the shortest execution time. Compared with the SOGGDD detector, our proposed method is approximately 25 times faster. It can also be found from Table 9 that our proposed method meets the requirement of real-time processing. It is worth to note

This article has been accepted for publication in a future issue of this journal, but has not been fully edited. Content may change prior to final publication. Citation information: DOI 10.1109/ACCESS.2020.3032751, IEEE Access

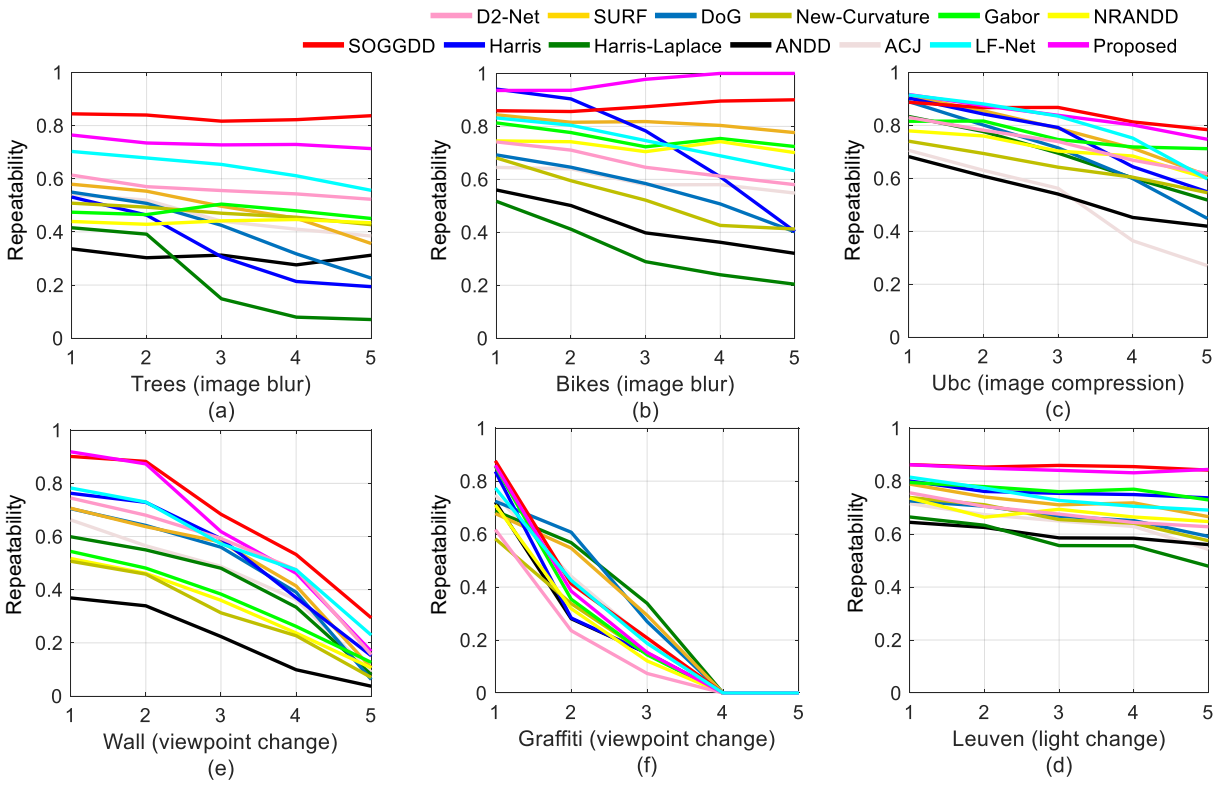

FIGURE 11. Average repeatability of different interest point detectors on six image scenes.

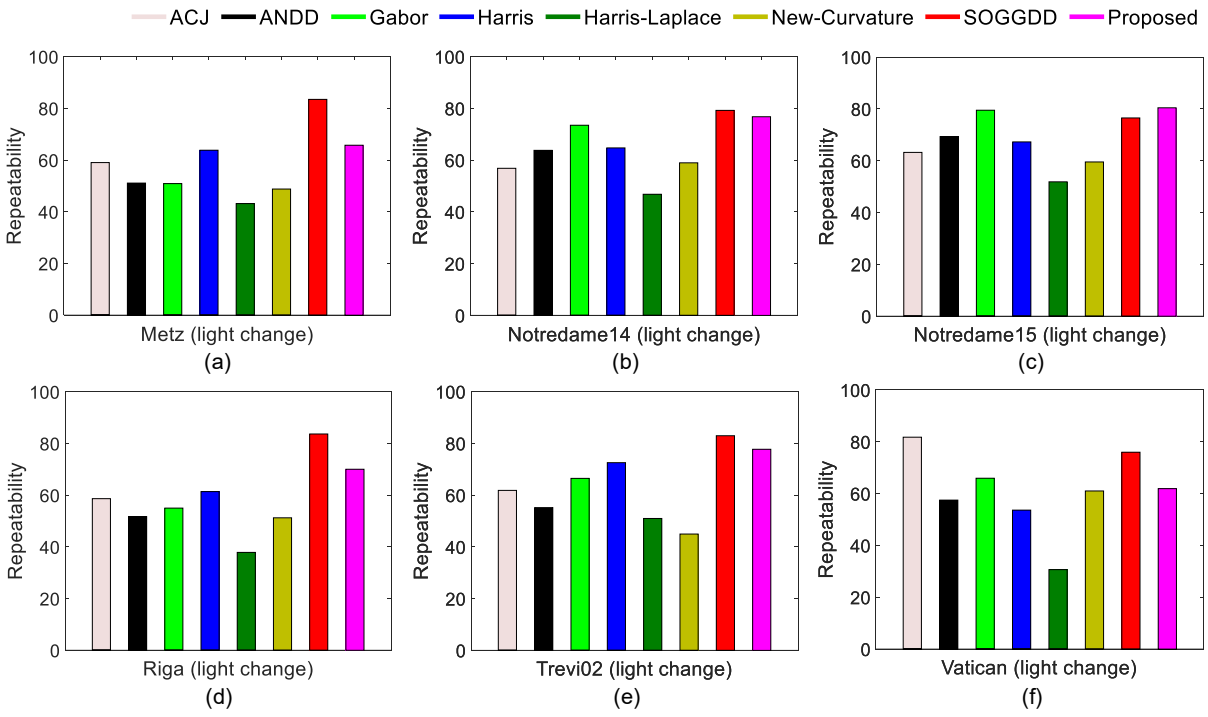

FIGURE 12. Average repeatability of different corner detectors on six image scenes.

This article has been accepted for publication in a future issue of this journal, but has not been fully edited. Content may change prior to final publication. Citation information: DOI 10.1109/ACCESS.2020.3032751, IEEE Access

TABLE 9. Performance comparison for the eight detectors on execution time (s).

Method	image						
	'Block'	'Polygon'	'Lab'	'Checkerboard'	'Boat'	'Bikes'	'Tree'
	(256 × 256)	(256 × 256)	(512 × 512)	(540 × 420)	(850 × 680)	(1000 × 700)	(700 × 1000)
Harris	0.102	0.115	0.424	0.397	0.951	1.172	1.212
ACJ	0.629	0.258	1.994	0.786	10.036	9.887	15.846
Harris-Laplace	0.108	0.118	0.431	0.597	1.514	1.864	1.945
ANDD	0.872	0.570	4.537	1.718	11.186	6.294	11.168
NRANDD	0.092	0.218	0.393	0.459	2.246	1.048	8.339
Gabor	0.912	0.691	5.253	1.943	14.350	9.137	17.676
SOGGDD	1.984	2.178	8.142	7.337	22.135	35.369	35.789
Proposed	**0.085**	**0.098**	**0.358**	**0.293**	**0.776**	**0.842**	**0.820**

TABLE 7. Average result for repeatability under overlap rate.

Detector	Image						ALL
	Trees	Bikes	Ubc	Leuven	Wall	Graffiti	
Harris	0.342	0.728	0.746	0.760	0.521	0.254	0.559
Harris-Laplace	0.221	0.332	0.685	0.578	0.409	**0.319**	0.424
SOGGDD	**0.832**	0.877	**0.844**	**0.854**	**0.659**	0.299	**0.728**
DoG	0.405	0.566	0.691	0.668	0.412	0.320	0.510
SURF	0.487	0.812	0.776	0.725	0.489	0.304	0.599
ACJ	0.459	0.586	0.510	0.642	0.434	0.277	0.485
ANDD	0.308	0.428	0.540	0.600	0.214	0.230	0.390
New-Curvature	0.471	0.527	0.645	0.664	0.315	0.213	0.466
D2-Net	0.561	0.658	0.727	0.681	0.530	0.185	0.557
LF-Net	0.640	0.741	0.796	0.742	0.558	0.277	0.626
Gabor	0.475	0.758	0.762	0.767	0.360	0.271	0.570
NRANDD	0.438	0.727	0.705	0.681	0.336	0.230	0.520
Proposed	0.734	**0.970**	0.836	0.845	0.608	0.280	0.712

TABLE 8. Average result for repeatability under different lighting conditions.

Detector	Image sets						ALL
	Metz	N14	N15	Riga	Trevi02	Vatican	
ACJ	0.590	0.569	0.632	0.587	0.618	**0.818**	0.636
ANDD	0.511	0.638	0.693	0.517	0.552	0.575	0.581
Gabor	0.509	0.735	0.795	0.550	0.665	0.659	0.652
Harris	0.638	0.647	0.673	0.614	0.726	0.536	0.639
Harris-Laplace	0.432	0.468	0.519	0.379	0.510	0.307	0.436
New-Curvature	0.488	0.590	0.595	0.513	0.450	0.610	0.541
SOGGDD	**0.835**	**0.792**	0.765	**0.837**	**0.830**	0.760	**0.830**
Proposed	0.657	0.768	**0.804**	0.700	0.777	0.619	0.721

that our method is 23.3 times faster than the SOGGDD method when the image size is 256 × 256. When the image size is 700 × 1000, our method is 43.6 times faster than the SOGGDD detector. Therefore, when the image size increases, the acceleration effect of our proposed method will become more apparent.

IV. CONCLUSION

In this paper, a fast corner detection method is proposed which has the ability to meet the requirement of real-time processing and good corner detection performance. The integral image, box filter, and a new rough screening mechanism are utilized to obtain the second-order directional derivative from an input image for efficiently detecting corners. The experimental comparisons indicate that our proposed corner detection algorithm has the good performance of corner detection and the ability of real-time corner detection in light of six evaluation criteria (accuracy of corner detection, localization error, average repeatability under image affine transformation, region repeatability, different lighting conditions, and execution time). Furthermore, the proposed corner detection method has a great potential to be applied in object recognition, 3D reconstruction, and many other image processing and computer vision tasks.

Reference

[1] B. Fan, Q. Kong, X. Wang, Z. Wanga, S. Xiang, C. Pan, and P. Fua, "A performance evaluation of local features for image based 3D reconstruction," *IEEE Transactions on Image Processing*, vol. 28, no. 10, pp. 4774–4789, 2019.

[2] H. Huang, H. Zhou, H. Qin, and M. Sheng, "Underwater vehicle visual servo and target grasp control," in *Proceedings of the IEEE Conference on International Conference on Robotics and Biomimetics*, 2016, pp. 1619–1624.

[3] S. Lowry, N. Sünderhauf, P. Newman, J. J. Leonard, D. Cox, P. Corke, and M. J. Milford, "Visual place recognition: A survey," *IEEE Transactions on Robotics*, vol. 32, no. 1, pp. 1–19, 2015.

[4] J. Ma, J. Jiang, H. Zhou, J. Zhao, and X. Guo, "Guided locality preserving feature matching for remote sensing image registration," *IEEE Transactions on Geoscience and Remote Sensing*, vol. 56, no. 8, pp. 4435–4447, 2018.

[5] W. Zhang and C. Sun, "Corner detection using multi-directional structure tensor with multiple scales," *International Journal of Computer Vision*, vol. 128, no. 2, pp. 438–459, 2020.

[6] F. Mokhtarian and A. Mackworth, "Scale-based description and recognition of planar curves and two-dimensional shapes," *IEEE Transactions on Pattern Analysis and Machine Intelligence*, vol. 8, no. 1, pp. 34–43, 1986.

[7] F. Mokhtarian and R. Suomela, "Robust image corner detection through curvature scale space," *IEEE Transactions on Pattern Analysis and Machine Intelligence*, vol. 20, no. 12, pp. 1376–1381, 1998.

[8] X. He and N. H. C. Yung, "Corner detector based on global and local curvature properties," *Optical Engineering*, vol. 47, no. 5, pp. 057 008–1–057 008–12, 2008.

[9] M. Awrangjeb and G. Lu, "Robust image corner detection based on the chord-to-point distance accumulation technique," *IEEE Transactions on Multimedia*, vol. 10, no. 6, pp. 1059–1072, 2008.

[10] W.-C. Zhang and P.-L. Shui, "Contour-based corner detection via angle difference of principal directions of anisotropic Gaussian directional derivatives," *Pattern Recognition*, vol. 48, no. 9, pp. 2785–2797, 2015.

[11] W. Zhang, C. Sun, T. Breckon, and N. Alshammari, "Discrete curvature representations for noise robust image corner detection," *IEEE Transactions on Image Processing*, vol. 28, no. 9, pp. 4444–4459, 2019.

[12] S. M. Smith and J. M. Brady, "SUSAN: A new approach to low level image processing," *International Journal of Computer Vision*, vol. 23, no. 1, pp. 45–78, 1997.

[13] E. Rosten and T. Drummond, "Machine learning for high-speed corner detection," in *Proceedings of the European Conference on Computer Vision*, 2006, pp. 430–443.

[14] E. Rosten, R. Porter, and T. Drummond, "Faster and better: A machine learning approach to corner detection," *IEEE Transactions on Pattern Analysis and Machine Intelligence*, vol. 32, no. 1, pp. 105–119, 2010.

[15] G. S. Xia, J. Delon, and Y. Gousseau, "Accurate junction detection and characterization in natural images," *International Journal of Computer Vision*, vol. 106, no. 1, pp. 31–56, 2014.

[16] H. Moravec, "Visual mapping by a robot rover," in *Proceedings of the International Joint Conference on Artificial Intelligence*, vol. 1, 1979, pp. 598–600.

[17] C. Harris and M. Stephens, "A combined corner and edge detector," *Alvey Vision Conference*, vol. 15, no. 50, pp. 147–151, 1988.

[18] T. Lindeberg, "Detecting salient blob-like image structures and their scales with a scale-space primal sketch: A method for focus-of-attention," *International Journal of Computer Vision*, vol. 11, no. 3, pp. 283–318, 1993.

[19] D. G. Lowe, "Distinctive image features from scale-invariant keypoints," *International Journal of Computer Vision*, vol. 60, no. 2, pp. 91–110, 2004.

[20] H. Bay, A. Ess, T. Tuytelaars, and L. Van Gool, "Speeded-up robust features (SURF)," *Computer Vision and Image Understanding*, vol. 110, no. 3, pp. 346–359, 2008.

[21] P. F. Alcantarilla, A. Bartoli, and A. J. Davison, "KAZE features," in *Proceedings of the European Conference on Computer Vision*, 2012, pp. 214–227.

[22] Y. Cho, D. Kim, S. Saeed, M. U. Kakli, S.-H. Jung, J. Seo, and U. Park, "Keypoint detection using higher order Laplacian of Gaussian," *IEEE Access*, vol. 8, pp. 10 416–10 425, 2020.

[23] M. A. Duval-Poo, F. Odone, and E. De Vito, "Edges and corners with shearlets," *IEEE Transactions on Image Processing*, vol. 24, no. 11, pp. 3768–3780, 2015.

[24] M. A. Duval-Poo, N. Noceti, F. Odone, and E. De Vito, "Scale invariant and noise robust interest points with shearlets," *IEEE Transactions on Image Processing*, vol. 26, no. 6, pp. 2853–2867, 2017.

[25] E. Cuevas, M.-A. Díaz-Cortes, and E. Mezura, "Corner detection of intensity images with cellular neural networks (CNN) and evolutionary techniques," *Neurocomputing*, vol. 347, no. 28, pp. 82–93, 2019.

[26] Z. Zhao, B. Li, L. Chen, M. Xin, F. Gao, and Q. Zhao, "Interest point detection method based on multi-scale Gabor filters," *IET Image Processing*, vol. 13, no. 12, pp. 2098–2105, 2019.

[27] W. Zhang and C. Sun, "Corner detection using second-order generalized Gaussian directional derivative representations," *IEEE Transactions on Pattern Analysis and Machine Intelligence*, pp. 1–12, 2019.

[28] J. Canny, "A computational approach to edge detection," *IEEE Transactions on Pattern Analysis and Machine Intelligence*, vol. 8, no. 6, pp. 679–698, 1986.

[29] P.-L. Shui and W.-C. Zhang, "Noise-robust edge detector combining isotropic and anisotropic Gaussian kernels," *Pattern Recognition*, vol. 45, no. 2, pp. 806–820, 2012.

[30] W. C. Zhang, Y. L. Zhao, T. P. Breckon, and L. Chen, "Noise robust image edge detection based upon the automatic anisotropic Gaussian kernels," *Pattern Recognition*, vol. 63, pp. 193–205, 2017.

[31] R. Su, C. Sun, and T. D. Pham, "Junction detection for linear structures based on Hessian, correlation and shape information," *Pattern Recognition*, vol. 45, no. 10, pp. 3695–3706, 2012.

[32] N. Xue, G.-S. Xia, X. Bai, L. Zhang, and W. Shen, "Anisotropic scale junction detection and matching for indoor images," *IEEE Transactions on Image Processing*, vol. 27, no. 1, pp. 78–91, 2017.

[33] K. Mikolajczyk and C. Schmid, "Scale and affine invariant interest point detectors," *International Journal of Computer Vision*, vol. 60, no. 1, pp. 63–86, 2004.

[34] X. Gao, F. Sattar, and R. Venkateswarlu, "Multiscale corner detection of gray level images based on LoG-Gabor wavelet transform," *IEEE Transactions on Circuits and Systems for Video Technology*, vol. 17, no. 7, pp. 868–875, 2007.

[35] M. Wang, W. Zhang, C. Sun, and A. Sowmya, "Corner detection based on shearlet transform and multi-directional structure tensor," *Pattern Recognition*, vol. 103, p. 107299, 2020.

[36] T. Hong-Phuoc and L. Guan, "A novel key-point detector based on sparse coding," *IEEE Transactions on Image Processing*, vol. 29, pp. 747–756, 2020.

[37] Y. Verdie, K. M. Yi, P. Fua, and V. Lepetit, "TILDE: A temporally invariant learned detector," in *Proceedings of the IEEE Conference on Computer Vision and Pattern Recognition*, 2015, pp. 5279–5288.

[38] K. M. Yi, E. Trulls, V. Lepetit, and P. Fua, "LIFT: Learned invariant feature transform," in *Proceedings of the European Conference on Computer Vision*, 2016, pp. 467–483.

[39] K. Lenc and A. Vedaldi, "Learning covariant feature detectors," in *Proceedings of the European Conference on Computer Vision*, 2016, pp. 100–117.

[40] Y. Ono, E. Trulls, P. Fua, and K. M. Yi, "LF-Net: Learning local features from images," in *Proceedings of the Advances in Neural Information Processing Systems*, 2018, pp. 6234–6244.

[41] M. Dusmanu, I. Rocco, T. Pajdla, M. Pollefeys, J. Sivic, A. Torii, and T. Sattler, "D2-Net: A trainable CNN for joint description and detection of local features," in *Proceedings of the IEEE Conference on Computer Vision and Pattern Recognition*, 2019, pp. 8092–8101.

[42] K. Mikolajczyk, T. Tuytelaars, C. Schmid, A. Zisserman, J. Matas, F. Schaffalitzky, T. Kadir, and L. Van Gool, "A comparison of affine region detectors," *International Journal of Computer Vision*, vol. 65, no. 1-2, pp. 43–72, 2005.

[43] P. Viola and M. Jones, "Rapid object detection using a boosted cascade of simple features," in *Proceedings of the IEEE conference on Computer Vision and Pattern Recognition*, vol. 1, 2001, pp. 511–518.

[44] F. Hu, G.-S. Xia, J. Hu, and L. Zhang, "Transferring deep convolutional neural networks for the scene classification of high-resolution remote sensing imagery," *Remote Sensing*, vol. 7, no. 11, pp. 14 680–14 707, 2015.

[45] K. A. Collins, J. F. Kielkopf, K. G. Stassun, and F. V. Hessman, "AstroImageJ: Image processing and photometric extraction for ultra-precise astronomical light curves," *The Astronomical Journal*, vol. 153, no. 2, p. 77, 2017.

[46] P.-L. Shui and W.-C. Zhang, "Corner detection and classification using anisotropic directional derivative representations," *IEEE Transactions on Image Processing*, vol. 22, no. 8, pp. 3204–3218, 2013.

[47] W.-C. Zhang, F.-P. Wang, L. Zhu, and Z.-F. Zhou, "Corner detection using Gabor filters," *IET Image Processing*, vol. 8, no. 11, pp. 639–646, 2014.

[48] A. Vedaldi and B. Fulkerson, "VLFeat: An open and portable library of computer vision algorithms," http://www.vlfeat.org/, 2008.

[49] P. Kovesi, "Code of Harris corner detector," https://peterkovesi.com/matlabfns/, 2005.

[50] F. Mokhtarian, "Image corner detection through curvature scale space," http://www.ee.surrey.ac.uk/CVSSP/demos/corners/, 2001.

[51] F. Mokhtarian and F. Mohanna, "Performance evaluation of corner detectors using consistency and accuracy measures," *Computer Vision and Image Understanding*, vol. 102, no. 1, pp. 81–94, 2006.

[52] J. Deng, W. Dong, R. Socher, L.-J. Li, K. Li, and L. Fei-Fei, "ImageNet: A large-scale hierarchical image database," in *Proceedings of the IEEE Conference on Computer Vision and Pattern Recognition*, 2009, pp. 248–255.

[53] M. Awrangjeb, G. Lu, and C. S. Fraser, "Performance comparisons of contour-based corner detectors," *IEEE Transactions on Image Processing*, vol. 21, no. 9, pp. 4167–4179, 2012.

[54] D. C. Hauagge and N. Snavely, "Image matching using local symmetry features," in *Proceedings of the IEEE Conference on Computer Vision and Pattern Recognition*, 2012, pp. 206–213.

TIAN GAO received the BS degree from the Xi'an University of Technology in China and he is pursuing the Master degree with the School of Electronic and Information, Xi'an Polytechnic University, China. His research interests include computer vision, image processing, and machine learning.

JUNFENG JING received the MS degree in electrical engineering from Xi'an Polytechnic University in China and the PhD degree in mechatronic engineering from Xidian University in China. He is a professor at Xi'an Polytechnic University, China. His research interests include artificial intelligence, machine vision, image processing, pattern recognition, and industrial robot control.

CHAO LIU received the BS degree from the East China Jiaotong University in China and he is pursuing the Master degree with the School of Electronic and Information, Xi'an Polytechnic University, China. His research interests include machine learning, computer vision, and image processing.

WEICHUAN ZHANG received the MS degree in signal and information processing from the Southwest Jiaotong University in China and the PhD degree in signal and information processing in National Lab of Radar Signal Processing, Xidian University, China. He is a research fellow at Griffith University, QLD, Australia. His research interests include computer vision, image analysis, and pattern recognition. He is a member of the IEEE.

YONGSHENG GAO received the B.Sc. and M.Sc. degrees in electronic engineering from Zhejiang University, Hangzhou, China, in 1985 and 1988, respectively, and the Ph.D. degree in computer engineering from Nanyang Technological University, Singapore. He is currently a Professor with the School of Engineering and Built Environment, Griffith University, and the Director of ARC Research Hub for Driving Farming Productivity and Disease Prevention, Australia. He had been the Leader of Biosecurity Group, Queensland Research Laboratory, National ICT Australia (ARC Centre of Excellence), a consultant of Panasonic Singapore Laboratories, and an Assistant Professor in the School of Computer Engineering, Nanyang Technological University, Singapore. His research interests include smart farming, machine vision for agriculture, computer vision, pattern recognition, environmental informatics, and medical imaging.

CHANGMING SUN received his PhD degree in computer vision from Imperial College London, London, UK in 1992. He then joined CSIRO, Sydney, Australia, where he is currently a Principal Research Scientist carrying out research and working on applied projects. He is also a Conjoint Professor at the School of Computer Science and Engineering of the University of New South Wales. He has served on the program/organizing committees of various international conferences. He is an Associate Editor of the EURASIP Journal on Image and Video Processing. His current research interests include computer vision, image analysis, and pattern recognition.